

A simple solution to mitigate noise effects in time-redundant sequences of small baseline multi-look DInSAR interferograms

Y. YANG^{†‡}, A. PEPE[‡], M. MANZO[‡], M. BONANO[‡], D. N. LIANG[†]
and R. LANARI^{*‡}

[†]School of Electronic Science and Engineering, National University of Defense
Technology, Changsha 410073, China

[‡]Istituto per il Rilevamento Elettromagnetico dell'Ambiente (IREA), Consiglio
Nazionale delle Ricerche (CNR), Napoli 80124, Italy

(Received 18 October 2012; in final form 28 January 2013)

We present a simple and effective filtering algorithm to mitigate noise effects in a time-redundant sequence of multi-look small baseline (SB) differential synthetic aperture radar (SAR) interferograms by exploiting the temporal relationships among the selected interferometric data pairs. The proposed method relies on the estimation of the (wrapped) filtered phase terms associated to each SAR acquisition; this result is achieved via a non-linear minimization procedure which is applied to the phase signal of conventional multi-look interferograms without any pixel selection process, and with no *a-priori* information on the statistics of the involved complex-valued SAR images. Following their estimation, the phase images are paired to reconstruct a new sequence of filtered SB differential interferograms, which are used to generate surface deformation products, such as deformation velocity maps and displacement time-series. The filtering algorithm effectiveness is demonstrated by analysing a set of SAR images acquired by the ENVISAT sensor from 2003 to 2010 over the city of Shanghai, China.

1. Introduction

Differential synthetic aperture radar (SAR) interferometry (DInSAR) represents nowadays a well-established remote sensing technique that allows detecting and monitoring, on large areas, earth surface deformation phenomena with centimetre to millimetre accuracy (Gabriel *et al.* 1989). This is done by exploiting the phase difference of SAR data pairs collected at different epochs and with slightly different looking angles. DInSAR measurements are usually corrupted by noise (decorrelation) due to thermal effects, baseline geometry and temporal changes (Zebker and Villasenor 1992), which can limit the use of the DInSAR technique for the analysis of geophysical phenomena. When dealing with sequences of SAR images, the decorrelation effects can be mitigated by selecting, among all the possible interferometric data pairs, only those characterized by small spatial and temporal separations (baselines). In addition, to mitigate decorrelation in the computed interferograms and to reduce the amount of data to be processed, complex multi-look (Rosen *et al.* 2000) and additional noise-filtering (Goldstein and Werner 1998, Baran *et al.* 2003) operations are also typically

*Corresponding author. Email: lanari.r@irea.cnr.it

carried out for each SAR interferogram. Notwithstanding, the differential interferograms that can be generated by applying these steps can still exhibit a high degree of phase noise.

To further improve the phase quality of the computed DInSAR interferograms, we propose in this work a simple filtering strategy that significantly lowers the phase noise affecting a sequence of time-redundant multi-look small baseline (SB) differential SAR interferograms, by exploiting their temporal relationships. The presented approach allows the retrieval of the (wrapped) filtered phases associated to each SAR acquisition that are then used to reconstruct a set of corresponding noise-filtered differential interferograms. Note that, at variance with other multi-temporal interferogram filtering techniques (Ferretti *et al.* 2011, Parizzi and Brcic 2011), the proposed approach is applied to conventional multi-look interferograms with no need to implement a pixel-by-pixel adaptive procedure carried out at the full spatial resolution grid, and aimed at preliminarily identifying distributed scatterers (DS). Moreover, it is straightforwardly carried out by solving a non-linear minimization problem relying on phase information only, without any *a-priori* assumption on the statistics of the exploited complex-valued SAR images (Monti Guarnieri and Tebaldini 2008). The performance of the proposed approach is investigated by using an ENVISAT SAR dataset acquired over the Chinese Yangtze Delta region, including the city of Shanghai, China, from 2003 to 2010. The achieved results demonstrate the effectiveness of the algorithm which may be used in various application contexts.

2. Interferogram noise-filtering algorithm

Let us consider a set of $N + 1$ SAR images collected at ordered epochs (t_0, t_1, \dots, t_N) , properly co-registered to a reference image, say the one acquired at t_m , with respect to which we also refer the temporal $\mathbf{T} \equiv [t_0 - t_m, \dots, t_N - t_m]^T$ and spatial $\mathbf{B}_\perp \equiv [b_{\perp 0}, b_{\perp 1}, \dots, b_{\perp N}]^T$ baseline vectors, the latter relevant to the perpendicular baseline component with respect to the radar line of sight (referred to as perpendicular baseline). From these SAR data, in order to limit the decorrelation noise artefacts, we compute a set of M small baseline multi-look DInSAR interferograms, namely $\Delta\Phi = [\Delta\Phi_1, \Delta\Phi_2, \dots, \Delta\Phi_M]^T$, simply selected by imposing thresholds on the maximum allowed temporal and perpendicular baseline values of the SAR data pairs (Berardino *et al.* 2002, Lanari *et al.* 2007). Furthermore, the computed interferograms can be profitably filtered by using one of the currently available noise-filtering approaches based on space and/or frequency analyses (Goldstein and Werner 1998, Baran *et al.* 2003). Note that this filtering step applied to the single interferograms is beneficial but not essential for the implementation of the technique discussed in the following, which could also directly start from the multi-look interferograms.

The proposed algorithm arises from the observation (Pepe and Lanari 2006, Pepe 2009, Ferretti *et al.* 2011) that the generated (wrapped) multi-look interferograms are not fully time-consistent because the multi-look operations (and, if implemented, also the additional noise-filtering steps) are independently carried out on each single interferometric data pair. Indeed, the sum of three multi-look interferograms computed from the SAR images acquired at the generic epochs, t_A , t_B and t_C , namely $\Delta\Phi_{BA} = \langle \Phi(t_B) - \Phi(t_A) \rangle_{-\pi, \pi}$, $\Delta\Phi_{CB} = \langle \Phi(t_C) - \Phi(t_B) \rangle_{-\pi, \pi}$ and $\Delta\Phi_{AC} = \langle \Phi(t_A) - \Phi(t_C) \rangle_{-\pi, \pi}$, is different from zero:

$$\langle \Delta\Phi_{BA} + \Delta\Phi_{CB} + \Delta\Phi_{AC} \rangle_{-\pi, \pi} \neq 0, \quad (1)$$

wherein the symbol $\langle \cdot \rangle_{-\pi, \pi}$ stands for the wrapping operator and $\Phi = [\Phi_0, \Phi_1, \dots, \Phi_N]^T$ is the vector of the unknown (wrapped) phase values related to each SAR acquisition. Our method allows the compensation of such temporal inconsistencies by computing the (unknown) phase vector Φ (associated with the SAR acquisitions) that is then used to reconstruct a new sequence of filtered, time-consistent interferograms. This result is achieved starting from multi-look DInSAR interferograms, which allow us reducing the amount of data to be processed and represent nowadays conventional products, routinely generated through the available scientific and commercial DInSAR software packages. It is worth remarking that the use of conventional multi-look interferograms is a distinctive characteristic of the proposed approach with respect to previous solutions, which are based on constraining the analysis to distributed scatterers, identified through a pixel-by-pixel selection procedure performed on the full resolution complex SAR image spatial grid (Ferretti *et al.* 2011, Parizzi and Brcic 2011). This selection permits to rely on the distributed scattering hypothesis (which is met when no dominant scatterers, such as artificial objects, are present in the resolution cell, Bamler and Hartl (1998)) under which the probability density function of the complex-valued SAR image may be regarded as being a zero-mean multivariate circular normal distribution. Under this assumption, an appropriate maximum likelihood estimation step of the filtered phase values associated with each SAR acquisition can be implemented (Ferretti *et al.* 2011). Because in our approach we focus on conventional multi-look interferograms, with no need of a pixel selection step, we cannot rely on the validity of the above mentioned distributed scattering hypothesis. Accordingly, we here propose a different solution that, for each pixel of the multi-look grid, searches for the phase vector $\hat{\Phi}$ that minimizes the weighted circular variance, say $\xi(\cdot)$, of the residual phases, representing the differences between the original and reconstructed interferograms (Mardia and Jupp 2000, Brunson and Charlton 2006):

$$\xi(\hat{\Phi}) = 1 - \frac{\left| \sum_{k=1}^M w_k \exp(j\delta_k) \right|}{\sum_{k=1}^M w_k}, \quad (2)$$

where $j = \sqrt{-1}$, $\hat{\Phi} = [\hat{\Phi}_0, \hat{\Phi}_1, \dots, \hat{\Phi}_N]^T$ is the vector of the estimated (wrapped) phase values related to each SAR acquisition, and $\delta_k = \langle \Delta\Phi_k - \hat{\Phi}_{E_k} + \hat{\Phi}_{S_k} \rangle_{-\pi, \pi}$, $\forall k = 1, \dots, M$ are the residual phases, being $E = [E_1, E_2, \dots, E_M]^T$ and $S = [S_1, S_2, \dots, S_M]^T$ the two index vectors related to the master and slave time acquisitions of the selected SAR data pairs, respectively. Moreover, the weights w_k , $\forall k = 1, \dots, M$ represent the estimates of the spatial coherences computed from the phase of the original multi-look interferograms, as follows (Bamler and Hartl 1998):

$$w_k(x, r) = \frac{1}{(N_A + 1)(N_R + 1)} \left| \sum_{h=-N_A/2}^{N_A/2} \sum_{p=-N_R/2}^{N_R/2} \exp[j\Delta\Phi_k(x+h, r+p)] \right| \quad \forall k = 1, \dots, M, \quad (3)$$

where $N_A + 1$ and $N_R + 1$ are the number of azimuth and range pixels within the used boxcar averaging window, centred around the generic pixel of coordinates (x, r) .

Additional considerations are now in order. First, we remark that in our analysis we use only small perpendicular and temporal baseline interferograms because the large baseline ones do not contribute with relevant information in equation (2), since the corresponding $w_k(\cdot)$ values are very small (Zebker and Villasenor 1992). Second, we underline that the minimization of the non-linear functional in (2) can be performed by using one of the several non-linear optimization routines available in literature (Kirkpatrick *et al.* 1983, Zhu *et al.* 1997, Waltz *et al.* 2006). In particular, in this work we use the solver developed by Zhu *et al.* (1997), which implements a limited memory quasi-Newton approach that is particularly suitable to solve constrained/unconstrained large non-linear optimization problems, by guaranteeing stable results and high computational efficiency. Third, we observe that the factor $\Lambda(\cdot) = \left| \frac{\sum_{k=1}^M w_k \exp(j\delta_k)}{\sum_{k=1}^M w_k} \right|$ in equation (2) also represents a weighted version of the temporal coherence factor originally proposed in Pepe and Lanari (2006), and widely used in Small BAseline Subset (SBAS) (Berardino *et al.* 2002) analyses (Lanari *et al.* 2007, Manzo *et al.* 2012) as a quality index for the retrieved deformation time-series. Note also that the optimal values of $\Lambda(\cdot)$ in equation (2) can be adopted as a reliability measure of the phase reconstruction. In particular, for pixels where $\Lambda(\cdot) \rightarrow 1$, we expect that reconstructed phases are almost identical to the original ones; on the other hand, very low values of $\Lambda(\cdot)$ correspond to a poor fit among the reconstructed and observed phase values.

Finally, once the $N + 1$ (wrapped) phase values are estimated, they are paired to retrieve the sequence of noise-filtered DInSAR interferograms, which can be subsequently used to generate surface deformation products through advanced DInSAR approaches (Sandwell and Price 1998, Berardino *et al.* 2002, Mora *et al.* 2003). We also underline that, even though the proposed algorithm is intrinsically small baseline-oriented, at this stage, not only SB interferograms but, in principle, any interferogram can be reconstructed.

3. Experimental results

We investigate the effectiveness of the proposed filtering algorithm by using a SAR dataset composed by 49 radar images acquired over ascending orbits (track 497, frame 616) by the ENVISAT satellite from 2003 to 2010, which can be represented in the temporal/perpendicular baseline plane as shown in figure 1.

The test-site area, extending for about $100 \text{ km} \times 100 \text{ km}$, encompasses the Yangtze Delta region (China) and includes Shanghai, one of the largest world's megacities, which has been affected by severe land subsidence phenomena, mainly due to anthropogenic factors such as the withdrawal of water from underground and the massive construction of high-rise buildings (Shi and Bao 1984, Liu *et al.* 2008). The presented DInSAR analysis exploits a sequence of SB time-redundant differential interferograms, selected by limiting the maximum perpendicular baseline and the relevant time span of the SAR data pairs to 400 m and 2000 days, respectively. Note that these threshold values have been derived through extensive experimental analyses carried out in several geophysical contexts by exploiting the SBAS approach (Lanari *et al.* 2007 and references therein, Manzo *et al.* 2012 and references therein). As a result, we retrieved a network of 664 differential SAR interferograms (see figure 1), which were computed by performing a complex multi-look operation with 4 looks in the range direction and 20 looks in the azimuth one (Bamler and Hartl 1998, Rosen *et al.*

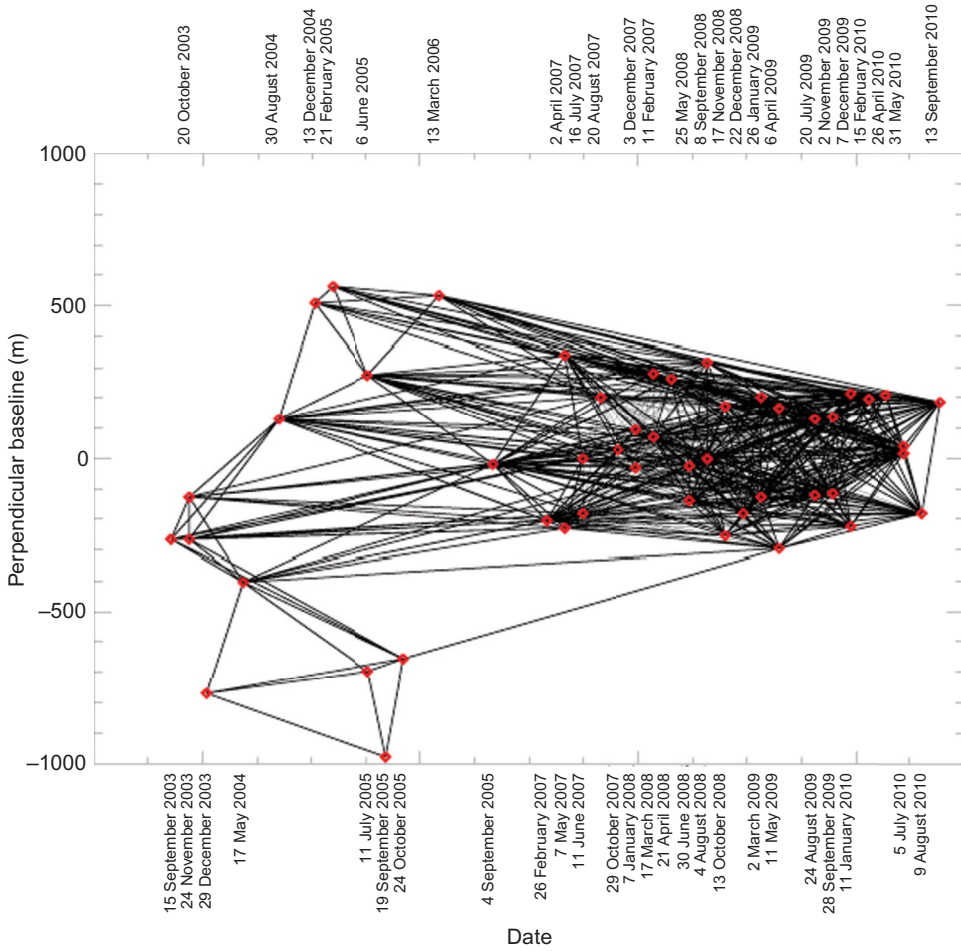


Figure 1. SAR data distribution in the temporal/perpendicular baseline plane. Red diamonds: SAR acquisition dates; black lines: interferograms used within the proposed noise-filtering approach.

2000, Lanari *et al.* 2007), leading to a resulting pixel dimension of about $100 \text{ m} \times 100 \text{ m}$. For the interferogram generation (Gabriel *et al.* 1989), the topographic phase contributions were removed by using precise satellite orbit information and a three-arcsecond shuttle radar topography mission (SRTM) digital elevation model (DEM) of the region. The multi-look interferograms were also pre-filtered by applying the well-known approach described in Goldstein and Werner (1998), and subsequently processed by following the lines of the filtering approach described in the previous section.

To investigate the algorithm performance in different spatial coherence conditions, we show in figure 2 some examples relevant to SAR data pairs belonging to three distinctive groups of DInSAR interferograms, selected according to their perpendicular and temporal baselines. In particular, the fringes depicted on the left side of figure 2 represent a selection of original interferograms after multi-look operation and additional noise-filtering based on Goldstein and Werner (1998), whereas

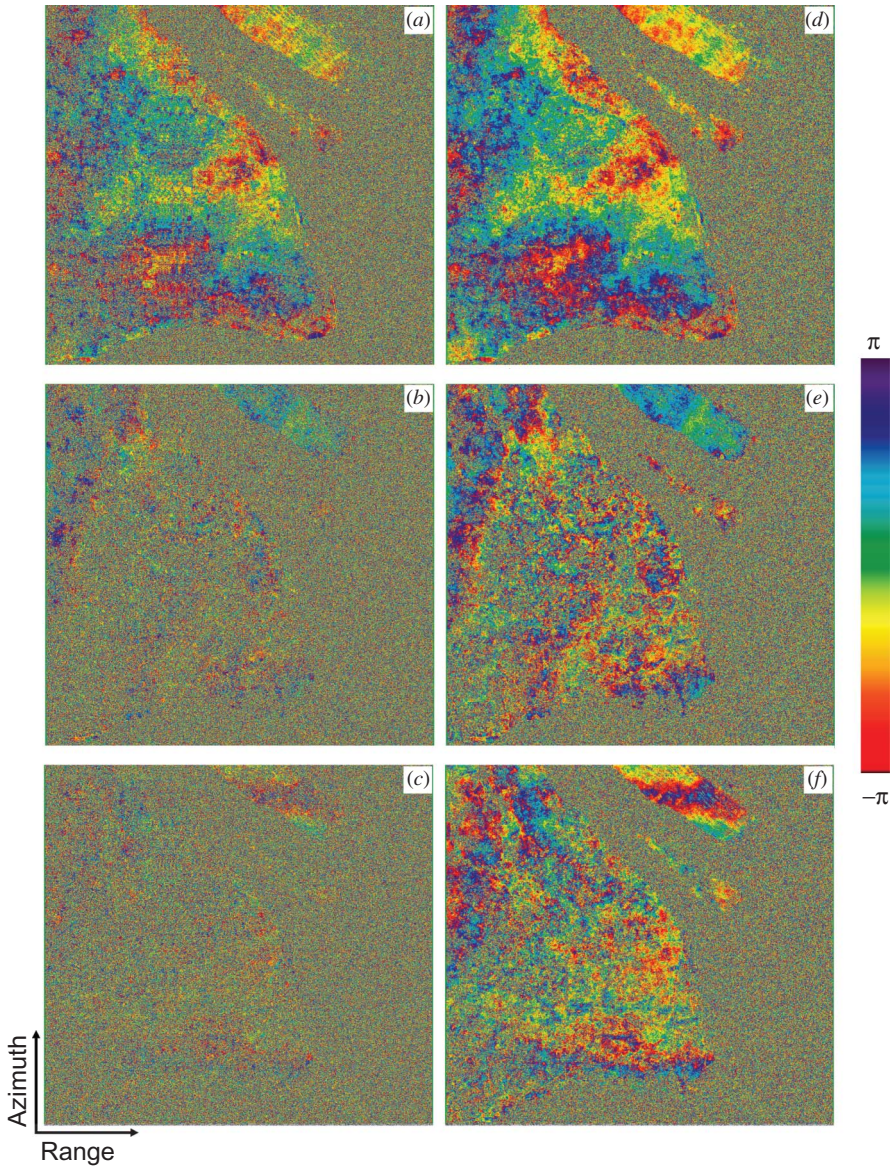


Figure 2. Comparison between original (left column) and noise-filtered (right column) multi-look interferograms. (a), (b), (c) 11 June 2007–20 August 2007, 26 February 2007–09 August 2010 and 11 June 2007–13 September 2010 SAR interferograms, with perpendicular baseline values of 378 m, 24 m, and 363 m, respectively. Note that the original interferograms were pre-filtered by using the Goldstein and Werner (1998) approach with a power coefficient equal to 0.5. (d), (e), (f). Reconstructed multi-look interferograms corresponding to the ones in (a), (b), (c), respectively.

on the right side we portray the corresponding reconstructed fringes. By comparing the homologous interferograms of figure 2, it is evident the effectiveness of the proposed algorithm. Moreover, we observe that the decorrelation effects, clearly visible in the interferograms shown in figures 2(b) and (c), characterized by large

temporal baselines, are particularly relevant. To further confirm the validity of the proposed method, we also compute the spatial coherence related to both the original $\Delta\Phi$ and reconstructed $\Delta\hat{\Phi} = \hat{\Phi}_E - \hat{\Phi}_S$ interferograms, being $\hat{\Phi}_E = [\hat{\Phi}_{E_1}, \hat{\Phi}_{E_2}, \dots, \hat{\Phi}_{E_M}]^T$ and $\hat{\Phi}_S = [\hat{\Phi}_{S_1}, \hat{\Phi}_{S_2}, \dots, \hat{\Phi}_{S_M}]^T$ the retrieved phase vectors corresponding to the master and slave SAR acquisitions of the selected SAR data pairs, the latter obtained from equation (3) where $\Delta\Phi$ is now replaced by $\Delta\hat{\Phi}$. In figures 3(a) and (b) we show the coherence maps relevant to the original and the reconstructed interferograms, respectively.

The two maps clearly show how the number of coherent pixels increases when moving from the original interferograms to the reconstructed ones. Moreover, we emphasize this spatial coherence improvement by comparing in figure 3(c) the histograms of the two spatial coherence maps; again, the obtained enhancement is clear. Finally, to highlight the spatial coherence improvement for each SAR data pair, we report in figure 3(d) the difference of the coherent pixel number between filtered and

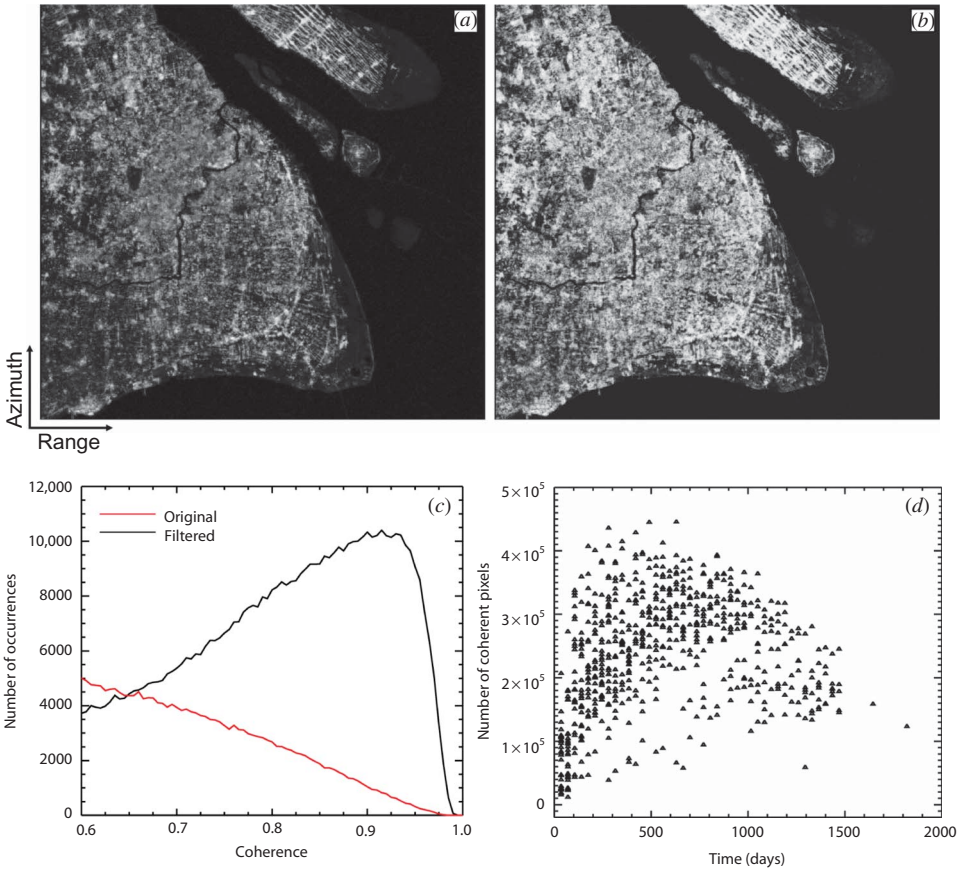


Figure 3. Radar filtering performance assessment. (a), (b) Coherence maps of original and reconstructed interferograms, respectively. (c) Histograms of the coherence maps, the red line refers to results shown in figure 3(a) and the black line to the ones presented in figure 3(b). (d) Difference between the total number of coherent pixels (coherence threshold equal to 0.6) for the filtered and the original interferograms, plotted w.r.t. the SAR data pair temporal baseline.

original interferograms, plotted w. r. t. the temporal baseline of the SAR data pairs. Note that the coherent pixels are those for which the average spatial coherence values are larger than 0.6. It is clear that the improvement of the spatial coherence is larger for ‘moderately low’ temporal baseline values while it tends to decrease as the temporal baselines increase.

As said before, the computed noise-filtered interferograms can be used to perform DInSAR analyses by exploiting one of the currently available multi-temporal DInSAR processing approaches. In particular, we apply in this work a simple strategy to investigate the displacements affecting the study area. To this aim, after performing the phase unwrapping step on each filtered interferogram (Costantini and Rosen 1999), we estimate, for each coherent pixel, the mean deformation velocity, namely v , along with possible topographic artefacts, namely Δz , by simply searching for the least squares solution of the following system of equations:

$$\Delta\Psi_k = \frac{4\pi}{\lambda} \left[\frac{\Delta b_{\perp k}}{r \sin \vartheta} \Delta z + v \Delta t_k \right], \quad \forall k = 1, \dots, M, \quad (4)$$

where $\Delta\Psi_k$ is the k th unwrapped interferogram, λ is the transmitted wavelength, ϑ is the incidence angle, $\Delta t_k = t_{E_k} - t_{S_k}$ and $\Delta b_{\perp k} = b_{\perp E_k} - b_{\perp S_k}$ are the temporal and perpendicular baseline values of the k th interferogram, respectively, and r is the sensor-to-target distance. The computed 2003–2010 mean deformation velocity map, superimposed on the SAR multi-look amplitude image of the area, is shown in figure 4(a). This representation is visually effective and allows us to easily identify the areas subject to significant displacement phenomena. A distinctive deformation behaviour can be recognized in spotted areas, mainly disposed along the Yangtze River and in the downtown zone where subsidence phenomena are due to the variation of the groundwater table and/or to the action of overloads associated to the urban sprawl

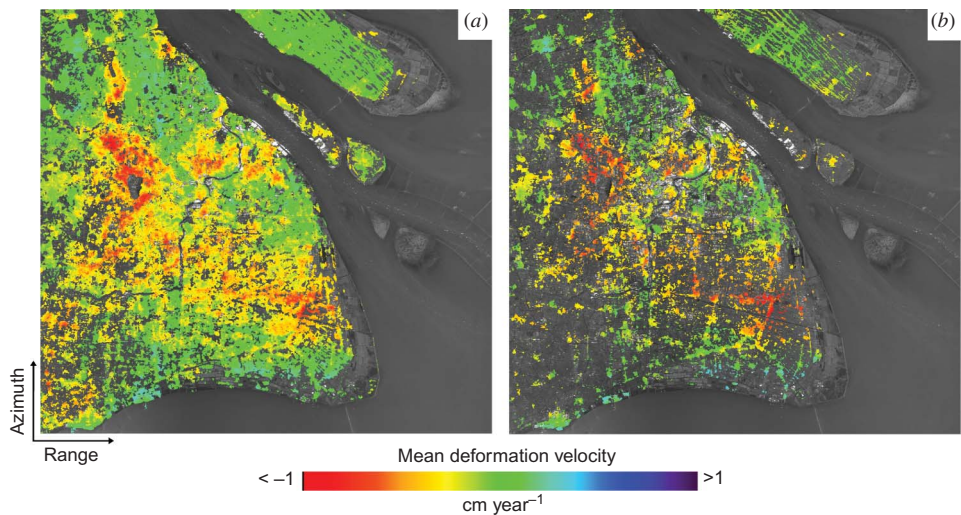


Figure 4. Mean deformation velocity maps of Chinese Yangtze Delta region, computed in coherent pixels only and superimposed on the SAR amplitude image (grayscale representation) of the zone, retrieved starting from (a) the noise-filtered interferograms and (b) the original ones, respectively.

(Liu *et al.* 2008). For the sake of comparison, we also show in figure 4(b) the mean deformation velocity map retrieved starting from the original interferograms. By comparing figures 4(a) and (b) it is clear the improvement of the spatial coverage as well as the possibility to deeper analyse the deformation phenomena affecting the study area while moving from the original to the noise-filtered interferograms.

4. Conclusions

We propose in this work a simple but effective approach to mitigate decorrelation noise effects in a sequence of time-redundant small baseline DInSAR interferograms by using their temporal relationships. The presented technique allows the computation of a set of noise-filtered interferograms, which is straightforwardly carried out by solving a non-linear minimization problem that only relies on the phase information of standard multi-look interferograms. In particular, the proposed approach does not need to implement any pixel selection procedure at the full spatial resolution scale and does not require the knowledge of *a-priori* information on the statistics of the involved complex-valued SAR images. Accordingly, it can be applied to conventional SB multi-look interferograms, which can be also profitably pre-filtered by using one of the available noise-filtering approaches based on space and/or frequency analyses to further improve noise-filtering performance. The effectiveness of the proposed approach has been demonstrated by analysing a set of real SAR data acquired by the ENVISAT sensor over the city of Shanghai, China, during the 2003–2010 time interval.

It is worth noting that the developed approach, being focused on SB multi-temporal, multi-look interferograms, is expected to be particularly suitable when applied for the generation of surface deformation time-series via the SBAS algorithm, which is a topic for future discussions.

Acknowledgements

We thank ESA for providing the SAR ENVISAT data within the Cat-1 Project No. 11461. Satellite orbit state vectors were provided by the University of Delft, The Netherlands. The DEM was from the NASA SRTM mission. This work was carried out under the sponsorship from the programme of China Scholarship Council CSC No. 2010611063.

References

- BAMLER, R. and HARTL, P., 1998, Synthetic aperture radar interferometry. *Inverse Problems*, **14**, pp. R1–R54.
- BARAN, I., STEWART, M.P., KAMPES, B.M., PERSKY, Z. and LILLY, P., 2003, A modification to the Goldstein radar Interferogram filter. *IEEE Transactions on Geoscience and Remote Sensing*, **41**, pp. 2114–2118.
- BERARDINO, P., FORNARO, G., LANARI, R. and SANSOSTI, E., 2002, A new algorithm for surface deformation monitoring based on small baseline differential SAR interferograms. *IEEE Transactions on Geoscience and Remote Sensing*, **40**, pp. 2375–2383.
- BRUNSDON, C. and CHARLTON, M., 2006, Local trend statistics for directional data – a moving window approach. *Computers, Environment and Urban Systems*, **30**, pp. 130–142.
- COSTANTINI, M. and ROSEN, P.A., 1999, A generalized phase unwrapping approach for sparse data. This is a paper presented at a conference. In *IGARSS 1999*, 28 June–2 July Hamburg, Germany, pp. 267–269.

- FERRETTI, A., FUMAGALLI, A., NOVALI, F., PRATI, C., ROCCA, F. and RUCCI, A., 2011, A new algorithm for processing interferometric data-stacks: SqueeSAR. *IEEE Transactions on Geoscience and Remote Sensing*, **49**, pp. 3460–3470.
- GABRIEL, A.K., GOLDSTEIN, R.M. and ZEBKER, H.A., 1989, Mapping small elevation changes over large areas: differential interferometry. *Journal of Geophysical Research*, **94**, pp. 9183–9191.
- GOLDSTEIN, R.M. and WERNER, C.L., 1998, Radar interferogram filtering for geophysical applications. *Geophysical Research Letters*, **25**, pp. 4035–4038.
- KIRKPATRICK, S., GELATT, C.D. and VECCHI, M.P., 1983, Optimization by simulated annealing. *Science*, **220**, pp. 671–680.
- LANARI, R., CASU, F., MANZO, M., ZENI, G., BERARDINO, P., MANUNTA, M. and PEPE, A., 2007, An overview of the Small BAseline Subset algorithm: a DInSAR technique for surface deformation analysis. *Pure and Applied Geophysics*, **164**, pp. 637–661.
- LIU, G.X., LUO, X.J., CHEN, Q., HUANG, D.F. and DING, X.L., 2008, Detecting land subsidence in Shanghai by PS-networking SAR interferometry. *Sensor*, **8**, pp. 4725–4741.
- MANZO, M., FIALKO, Y., CASU, F., PEPE, A. and LANARI, R., 2012, A quantitative assessment of DInSAR measurements of interseismic deformation: the Southern San Andreas fault case study. *Pure and Applied Geophysics*, **169**, pp. 1463–1482.
- MARDIA, K.V. and JUPP, P.E., 2000, *Directional Statistics*, 429 pp (New York: Wiley).
- MONTI GUARNIERI, A. and TEBALDINI, S., 2008, On the exploitation of target statistics for SAR interferometry applications. *IEEE Transactions on Geoscience and Remote Sensing*, **46**, pp. 3436–3443.
- MORA, O., MALLORQUÍ, J.J. and BROQUETAS, A., 2003, Linear and nonlinear terrain deformation maps from a reduced set of interferometric SAR images. *IEEE Transactions on Geoscience and Remote Sensing*, **41**, pp. 2243–2253.
- PARIZZI, A. and BRCIC, R., 2011, Adaptive InSAR stack multilooking exploiting amplitude statistics: a comparison between different techniques and practical results. *IEEE Geoscience and Remote Sensing Letters*, **8**, pp. 441–445.
- PEPE, A., 2009, *Advanced Differential Interferometric SAR Techniques, the Extended Minimum Cost Flow Phase Unwrapping (EMCF) Technique* (Saarbrücken: VDM Verlag), ISBN:978-3-639-19577-4.
- PEPE, A. and LANARI, R., 2006, On the extension of the minimum cost flow algorithm for phase unwrapping of multitemporal differential SAR interferograms. *IEEE Transactions on Geoscience and Remote Sensing*, **44**, pp. 2374–2383.
- ROSEN, P.A., HENSLEY, S., JOUGHIN, I.R., LI, F.K., MADSEN, S.R., RODRIGUEZ, E. and GOLDSTEIN, R.M., 2000, Synthetic aperture radar interferometry. *Proceedings of the IEEE*, **88**, pp. 333–382.
- SANDWELL, D.T. and PRICE, E.J., 1998, Phase gradient approach to stacking interferograms. *Journal of Geophysical Research*, **103**, pp. 30183–30204.
- SHI, L.X. and BAO, M.F., 1984, Case History No. 9.2: Shanghai, China. In *Guidebook to Studies of Land Subsidence due to Ground-water Withdrawal*, J.F. Poland (Ed.), pp. 155–160 (Paris: UNESCO).
- WALTZ, R.A., MORALES, J.L., NOCEDAL, J. and ORBAN, D., 2006, An interior algorithm for nonlinear optimization that combines line search and trust region steps. *Mathematical Programming*, **107**, pp. 391–408.
- ZEBKER, H.A. and VILLASENOR, J., 1992, Decorrelation in interferometric radar echoes. *IEEE Transactions on Geoscience and Remote Sensing*, **30**, pp. 950–959.
- ZHU, C., BYRD, R.H., LU, P. and NOCEDAL, J., 1997, L-BFGS-B: Fortran Subroutines for large-scale bound-constrained optimization. *Journal ACM Transactions on Mathematical Software (TOMS)*, **23**, pp. 550–560.